Cell Volume and Plasma Membrane Osmotic Water Permeability in Epithelial Cell Layers Measured by Interferometry

Javier Farinas and A. S. Verkman
Departments of Medicine and Physiology, Cardiovascular Research Institute, and Graduate Group in Biophysics, University of California, San Francisco, California 94143-0521 USA

ABSTRACT The development of strategies to measure plasma membrane osmotic water permeability (P_f) in epithelial cells has been motivated by the identification of a family of molecular water channels. A general approach utilizing interferometry to measure cell shape and volume was developed and applied to measure P_f in cell layers. The method is based on the cell volume dependence of optical path length (OPL) for a light beam passing through the cell. The small changes in OPL were measured by interferometry. A mathematical model was developed to relate the interference signal to cell volume changes for cells of arbitrary shape and size. To validate the model, a Mach-Zehnder interference microscope was used to image OPL in an Madin Darby Canine Kidney (MDCK) cell layer and to reconstruct the three-dimensional cell shape (OPL resolution $< \lambda/25$). As predicted by the model, a doubling of cell volume resulted in a change in OPL that was proportional to the difference in refractive indices between water and the extracellular medium. The time course of relative cell volume in response to an osmotic gradient was computed from serial interference images. To measure cell volume without microscopy and image analysis, a Mach-Zehnder interferometer was constructed in which one of two interfering laser beams passed through a flow chamber containing the cell layer. The interference signal in response to an osmotic gradient was analyzed to quantify the time course of relative cell volume. The calculated MDCK cell plasma membrane P_f of 6.1×10^{-4} cm/s at 24°C agreed with that obtained by interference microscopy and by a total internal reflection fluorescence method. Interferometry was also applied to measure the apical plasma membrane water permeability of intact toad urinary bladder; P_f increased fivefold after forskolin stimulation to 0.04 cm/s at 23°C. These results establish and validate the application of interferometry to quantify cell volume and osmotic water permeability in cell layers.

INTRODUCTION

The response of cell volume to osmotic gradients provides information about volume regulatory processes and the permeability of the cell plasma membrane to water and solutes. The recent identification of molecular water channels (Verkman et al., 1996; Nielsen and Agre, 1995) has motivated the search for direct quantitative methods to measure water permeability in various transfected cell models (Katsura et al., 1995) and native intact tissues (Folkesson et al., 1996). Although it is now established that water channels are widely expressed in epithelial and endothelial tissues that participate in vectorial fluid transport, a physiological need for water channels has been shown only for the kidney water channel AQP2, where mutations are associated with nephrogenic diabetes insipidus (Deen et al., 1994). Functional measurements of water permeability are important for analysis of the transporting properties of putative water channel proteins in heterologous expression systems and for the determination of water permeability in tissues expressing water channel proteins. In addition, functional measurements of water permeability will play a key role in the investigation of water transport mechanisms in transgenic knock-out mice lacking specific water channels.

Several experimental approaches have been applied to measure plasma membrane water permeability (P_f) in cell layers (reviewed in Verkman, 1995). In general, P_f is determined from the time course of relative cell volume in response to osmotic gradients. Light scattering has been used as a semiquantitative approach to infer cell volume changes in suspended cells and monolayers of adherent cultured cells (Echevarria and Verkman, 1992; Fischbarg et al., 1993); however, light scattering is suitable for a limited number of cell types in which the intensity of scattered light is sensitive to cell volume. In addition, it is difficult to determine P_f quantitatively because scattered light intensity depends on both the details of cell shape and the refractive indices of various cellular compartments. Other approaches have been developed to measure P_f in adherent cells based on measurement of the concentration of fluid-phase cytoplasmic fluorescent dyes. Relative cell volume is inferred from the inverse of the fluorophore concentration. Fluorophore concentration can be estimated by sampling the fluorescence signal from a restricted volume by partial confocal optics (Muallem et al., 1992) or by confocal microscopy (Crowe et al., 1995). However, it is difficult in small mammalian cells to generate a real-time signal from a slice of cytoplasm of thickness much smaller than cell height. We recently introduced a simple quantitative approach to determining fluorophore concentration based on total internal reflection (TIR) microfluorimetry (Farinas et al., 1995). The

Received for publication 16 July 1996 and in final form 23 September 1996.

Address reprint requests to Javier Farinas, Graduate Group in Biophysics, 1246 Health Sciences East Tower, University of California, San Francisco, CA 94143-0521. Tel.: 415-476-8530; Fax 415-665-3847; E-mail: javier@itsa.ucsf.edu.

0006-3495/96/12/3511/12 $2.00

steady-state fluorescence signal measured in the evanescent field (50–200 nm) produced by TIR excitation was inversely proportional to cell volume. The TIR fluorescence method is suitable for measuring relative cell volume in cells grown or immobilized on a homogeneous transparent support. Measurements in nonadherent cell sheets or intact tissues are not possible with these techniques, nor is the determination of cell shape or absolute cell volume.

The purpose of this study was to apply interferometry to quantify cell shape and water permeability in adherent and nonadherent cell layers. The principle of the method is shown schematically in Fig. 1. Light passing through a flow chamber containing a cell layer passes through two media with different refractive indices: the perfusate (n_p) and the cell (n^o_{cell}) (Fig. 1, *left*). The phase of the electric field vector of a light beam emerging from the chamber is shifted relative to that of the incident beam by an amount that depends on the optical path length. The total optical path length (OPL) is the sum of the OPL in each medium: OPL = $\Sigma h_i n_i$, where h_i is the geometric path length in medium i and n_i is the corresponding refractive index. As the cell volume changes, there is a change in the geometric path length of each medium as well as in the cell refractive index, resulting in a change in OPL. Because n_{cell} is proportional to the concentration of solutes in the cytoplasm (and thus proportional to inverse cell volume), the OPL for a swollen cell is equivalent to the OPL for a hypothetical cell consisting of the original cell plus that for a layer of water (n_w) (Fig. 1, *right*). The difference in OPL before versus after cell swelling is in this hypothetical "water" layer; initially the refractive index in this layer is that of the perfusate, whereas after swelling the refractive index is that of water. As shown below, the change in OPL is equal to the change in cell height multiplied by the difference in refractive indices between water and the perfusate. Thus the phase of the light beam emerging from the flow chamber will depend on cell volume. This small change in phase is measurable by interferometry as a change in interference signal amplitude. Furthermore, by using interference microscopy and image analysis, it is shown that cell shape can be reconstructed. Interferometry thus represents a simple and general approach to measuring the relative cell volume of adherent or nonadherent cell layers of arbitrary shape and size. This report validates and applies interferometry to the measurement of water permeability in MDCK cell layers and the epithelium of intact toad urinary bladder.

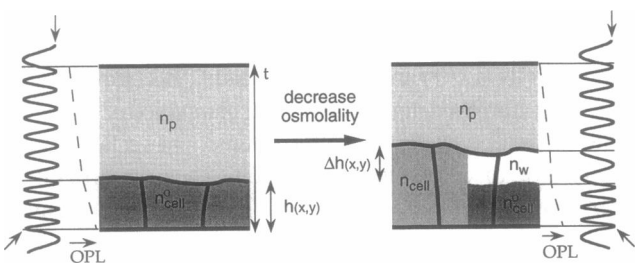

FIGURE 1 Schematic of a cell layer showing that optical path length (OPL) depends on cell volume. Initially, light passes through a flow chamber containing a cell layer and perfusate with refractive indices of n^o_{cell} and n_p, respectively. The phase of the light emerging from the chamber (*sinusoidal curve at left*) is shifted relative to the phase of the incident light by an amount that depends on the OPL (*dashed line*). A decrease in perfusate osmolality produces an increase in cell height [$\Delta h(x,y)$]. Because n_{cell} is proportional to the solute concentration in the cytosol, the OPL for a swollen cell (*left half of swollen cell shown at right*) is equivalent to the OPL for a hypothetical cell consisting of the original cell plus a layer of water (n_w) (*right half of swollen cell shown at right*). The difference in OPL before versus after cell swelling is in this layer; initially the refractive index in this layer is that of the perfusate, and after swelling the refractive index is that of water. The difference in OPL results in a difference in the phase of the light emerging from the flow chamber (see *arrows*), as quantified by Eqs. 1–8.

INSTRUMENTATION AND EXPERIMENTAL PROCEDURES

Interference microscopy

A 5-mW diode laser (λ = 676 nm; Imatronic, Newbury Berks, England) was used as the light source for a Mach-Zehnder transmitted light interference microscope (Leitz, Wetzlar, Germany) (Fig. 2 *A*). The light was passed through a vibrating fiberoptic to reduce the speckle pattern for uniform illumination across the field of view. A beam-splitting prism (BS_1) produced reference (R) and sample (S) beams, which passed through matched pairs of condensers and 50× air objectives (numerical aperture 0.85). The cell layer was positioned in a flow chamber (Farinas et al., 1995) in the sample beam path. A stack of glass microscope slides that approximately matched the optical path length of the flow chamber was positioned in the reference beam. The beams were recombined by a beam-splitting prism (BS_2) to produce interference, so that OPL differences introduced in the sample beam (due to the cell layer) relative to the reference beam would alter the interference pattern. The path length difference between the sample and reference beams could be adjusted with a series of plane parallel plates to introduce a linear increase in OPL across the image and thus produce parallel interference fringes of adjustable width. The inhomogeneous cell sample caused deviations in the fringes. Interference images were recorded by a 14-bit cooled CCD camera (512 × 512 pixels) controlled by PMIS software (Photometrics, Tucson, AZ).

Mach-Zehnder interferometry

A 10 mW He-Ne laser (λ = 633 nm) was used as the light source for a Mach-Zehnder interferometer (Fig. 2 *B*). The laser beam was split by a beam splitter (BS_1) into reference (R) and sample (S) beams. The reference beam was attenuated by a neutral density filter (ND) and reflected by a mirror (M_2). The sample beam passed through a flow chamber containing the cell layer and was reflected by a mirror (M_1). The flow chamber contained a fluid-filled channel (15 mm long, 4 mm wide, 0.1 mm deep). The beams were recombined by the beam splitter (BS_2) to cause interference. The interferometer was adjusted to produce the zeroth-order interference fringe. The recombined beam was expanded with a Fluor 10× air objective (Nikon) so that the central region of the beam illuminated a PDA50 silicon photodetector (aperture 1 mm; ThorLabs, Newton, NJ) located 1.6 m from the sample. Photodetector current was digitized by a 12-bit analog-to-digital converter interfaced to a PC computer. Data were collected at rates of 1–5 Hz. Air currents and temperature gradients were minimized by enclosing the interferometer in a Lucite box. The temperature of the perfusate was controlled by an in-line stainless steel cooling coil (length 60 cm) just proximal to the flow chamber, which was immersed in a water bath. The interferometer was mounted on an RS1000 optical table (Newport, Irvine, CA) to minimize vibrations.

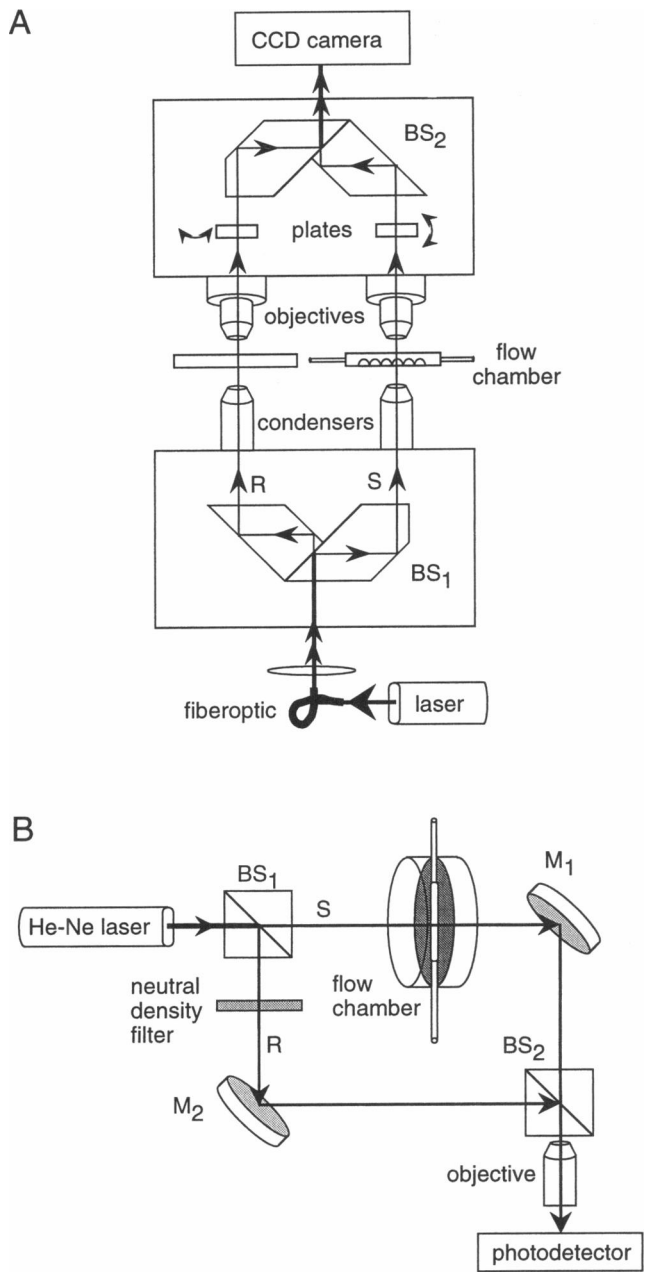

FIGURE 2 Schematic of interference microscope (*A*) and Mach-Zehnder interferometer (*B*). BS, beam splitter; R, reference beam; S, sample beam; M, mirror. See Instrumentation and Experimental Procedures for details.

Cells and epithelia

MDCK-1 cells (ATCC CCL no. 34; American Type Culture Collection, Rockville, MD) were cultured on 18-mm-diameter round glass coverslips in DME-H21 supplemented with 10% fetal calf serum, 100 units/ml penicillin and 100 milliunits/ml streptomycin. Cells were maintained at 37°C in a 95% air/5% CO_2 atmosphere. Urinary bladders from the toad *Bufo marinus* were dissected, washed, and mounted as hemibladder sacs as described previously (Shi et al., 1990). Bladders were incubated for 60 min in toad Ringer's solution at 23°C before experiments to eliminate any endogenous antidiuretic response. Bladder strips (2 cm × 2 cm) were cut and mounted with the apical membrane contacting the perfusate for water permeability measurements. The basolateral membrane was coated with immersion oil to prevent water transport across this membrane.

Solutions

Solutions consisted of phosphate-buffered saline (PBS) (in mM: 137 NaCl, 2.7 KCl, 1.5 KH_2PO_4, 8.1 Na_2HPO_4, pH 7.4, 300 mOsm), hypotonic PBS (PBS diluted 1:1 with deionized water, 150 mOsm), toad Ringer's (in mM: 110 NaCl, 2.5 $NaHCO_3$, 3 KCl, 2 KH_2PO_4, 1 $CaCl_2$, 5 glucose, pH 7.6, 240 mOsm), and hypotonic toad Ringer's (toad Ringer's diluted 1:1 with deionized water, 120 mOsm). Solution refractive indices, measured with an Abbe-3L refractometer (Milton Roy, Rochester, NY; precision 100 ppm), were equalized by the addition of a stock solution of 20% (w/v) dextran (MW 19,500; Sigma, St. Louis, MO). Equalization of refractive indices to within 20 ppm was achieved by adding dextran until the phase difference between solutions was undetectable as observed in the Mach-Zehnder interferometer with a 2-mm path length through the solutions.

THEORY AND DATA ANALYSIS

Relationship between optical path length and cell volume

For light passing perpendicular to a cell layer of height $h(x,y)$ and refractive index n_{cell}, within a flow chamber of depth D containing perfusate of refractive index n_p (Fig. 1), the optical path length (OPL) is

$$\begin{aligned} \mathrm{OPL}(x,y) &= [h(x,y)n_{cell} + \{D - h(x,y)\}n_p] \\ &= [h(x,y)(n_{cell} - n_p)] + \gamma', \end{aligned} \tag{1}$$

where γ' ($= Dn_p$) is the cell height-independent contribution to the optical path length. Because the refractive index of a solution, n, is generally proportional to solute concentration c ($n = n_o + [dn/dc]c$), it is assumed that in cells,

$$n_{cell} = n_w + (n^o_{cell} - n_w)(V_o/V), \tag{2}$$

where n_w is the refractive index of water and n^o_{cell} is the cell refractive index at volume V_o. Assuming that cells respond as perfect osmometers (ΠV = constant), where Π is the osmolality, Eq. 2 becomes

$$n_{cell} = n_w + (n^o_{cell} - n_w)(\Pi/\Pi_o). \tag{3}$$

If cell shape is assumed to remain constant during volume change (i.e., cell height is proportional to the original height profile, $h_o(x,y)$; $h(x,y) = h_o(x,y)(V/V_o)$), then Eqs. 1 and 2 can be combined to relate OPL to cell volume:

$$\mathrm{OPL}(x,y) = h_o(x,y)[(n_w - n_p)(V/V_o) + (n^o_{cell} - n_w)] + \gamma'. \tag{4}$$

As demonstrated qualitatively in Fig. 1, Eq. 4 indicates that optical path length is dependent on cell volume.

Interferometric measurement of OPL

The intensity $I(x,y)$ produced by the interference of a reference beam (not passing through cells) with electric field $E_r = E_{ro}\cos[\omega t - kr - \alpha]$, with the sample beam (passing through cells) with electric field $E_s = E_{so}\cos[\omega t - kr -$

$(2\pi/\lambda)$ OPL(x, y)] is (Hecht, 1987)

$$I(x, y) = \langle (E_r + E_s)^2 \rangle = E_{ro}^2/2 + E_{so}^2/2 + E_{ro}E_{so} \cos[(2\pi/\lambda)\mathrm{OPL}(x, y) - \alpha(x, y)], \quad (5)$$

where $\langle\ \rangle$ denotes the time average, $k = 2\pi/\lambda$, λ is wavelength, r is the distance along the beam axis, and $\alpha(x, y)$ is the relative phase difference of the reference beam and the sample beam without the sample. The value of $I(x, y)$ ranges between $I_{max} = (E_{ro}^2/2 + E_{so}^2/2 + E_{ro}E_{so})$ and $I_{min} = (E_{ro}^2/2 + E_{so}^2/2 - E_{ro}E_{so})$ and depends on the OPL difference between the sample and reference beams.

An interference microscope generates a map of $I(x, y)$ which, as shown below, can be used to generate a map of OPL(x, y). The integrated optical path length (Θ) is related to cell volume by integration of Eq. 4:

$$\Theta = \iint_{\text{cell}} \mathrm{OPL}(x, y)\, dx\, dy \Big/ \iint_{\text{cell}} dx\, dy = [(n_w - n_p)\, V + (n_{cell}^o - n_w)\, V_o + \Gamma]/A, \quad (6)$$

where Γ is a constant (integral of γ' over the cell) and A is the x, y-projected area of the cell. Equation 6 is valid even if cell volume change results in a change in cell shape.[1]

The constant Γ is related to the details of the flow chamber and is independent of cell volume. By measuring OPL(x, y) in areas of the image that do not contain cells, Γ is determined and subtracted from all values in the image. Equation 6 can be used to relate the difference in integrated optical path lengths $(\Theta - \Theta_o)$ to a change in cell volume $(V - V_o)$:

$$V - V_o = (n_w - n_p)^{-1}\, (\Theta - \Theta_o)A, \quad (7)$$

or to relate the ratio of integrated optical path lengths (Θ/Θ_o) to relative cell volume (V/V_o):

$$V/V_o = [(n_{cell}^o - n_p)/(n_w - n_p)/(n_w - n_p)] \cdot [\Theta/\Theta_o - (n_{cell}^o - n_w)/(n_{cell}^o - n_p)]. \quad (8)$$

When the spatially integrated intensity $[I_{si} = \iint_{\text{detector}} I(x, y)\, dx\, dy]$ is measured rather than $I(x, y)$ (as in Fig. 2 *B*), information is obtained on the OPL integrated over the cell layer. For a flat epithelium, the optical path length, L, is constant throughout the cell layer. Integrating Eq. 5 over x and y yields

$$I_{si} = a(E_{ro}^2/2 + E_{so}^2/2 + E_{ro}E_{so} \cos[(2\pi/\lambda)L - \alpha]), \quad (9)$$

where a is a conversion factor related to the detection system. Note that the cell height-independent phase difference α is a not a function of position because interference is recorded at the zeroth-order fringe. Equation 9 relates the measured integrated intensity to $(L - \alpha\lambda/2\pi)$ and thus to cell volume because

$$\begin{aligned} L - \alpha\lambda/2\pi &= h_o[(n_w - n_p)(V/V_o) + (n_{cell}^o - n_w)] + \gamma' - \alpha\lambda/2\pi \\ &= h_o[(n_w - n_p)(V/V_o)] - \alpha', \end{aligned} \quad (10)$$

where $\alpha' = \alpha\lambda/2\pi - \gamma' - h_o(n_{cell}^o - n_w)$ contains only volume-independent phase terms. It is shown in the Appendix that for a nearly flat epithelium (see Eq. A7),

$$I_{si} = E_{ro}^2/2 + E_{so}^2/2 + E_{ro}E_{so} \cos[(2\pi/\lambda)\Theta - \alpha], \quad (11)$$

whereas for an epithelium of arbitrary shape (see Eq. A9),

$$I_{si} = E_{ro}^2/2 + E_{so}^2/2[C^2 + S^2] + E_{ro}E_{so}[\cos(\alpha)\, C + \sin(\alpha)\, S], \quad (12)$$

where

$$C = \iint_{\text{cell}} \cos[(2\pi/\lambda)\mathrm{OPL}(x, y)]\, dx\, dy \Big/ \iint_{\text{cell}} dx\, dy,$$

and

$$S = \iint_{\text{cell}} \sin[(2\pi/\lambda)\mathrm{OPL}(x, y)]\, dx\, dy \Big/ \iint_{\text{cell}} dx\, dy.$$

With a specific model of cell shape, Eq. 11 or 12 relates the measured integrated intensity to cell volume change.

Conversion of interference images to optical path length maps

The observed interference image is related to the difference in optical path length introduced by the sample, OPL(x, y), and the microscope plane parallel plates $(\alpha(x, y) = a_x x + a_y y$, where a_x and a_y are the horizontal and vertical frequencies of the fringe pattern). To relate the interference image to cell volume, OPL(x, y) must be computed. Given an interference image I_{ij}, where i and j are row and column pixel indices, respectively, Eq. 5 can in principle be used to calculate a map of the differences in optical path length

[1] In imaging experiments, Eq. 6 can be derived independent of assumptions about cell shape change during volume change. For cells of arbitrary shape, Eq. 4 can be rewritten as

$$\mathrm{OPL}(x, y) = h(x, y)(n_w - n_p) + h_o(x, y)(n_{cell}^o - n_w + \gamma'.$$

The integrated optical path length (Θ) is related to cell volume by integration of OPL(x, y):

$$\Theta = \frac{\iint_{cell} \mathrm{OPL}(x, y)\, dx\, dy}{\iint_{cell} dx\, dy} = \frac{[(n_w - n_p)V + (n_{cell}^o - n_w)V_o + \Gamma]}{A}$$

where Γ is a constant (integral of γ' over the cell), and A is the x, y-projected area of the cell. Thus Eq. 6 is valid even if the cell volume change results in a change in cell shape.

between the sample and reference beams ($D_{ij} = OPL_{ij} - \alpha_{ij}\lambda/2\pi$). However, noise and nonuniform illumination will cause the intensity extrema, I_{min} and I_{max}, to be position dependent. An algorithm was developed that used the local intensity extrema together with Eq. 5 to calculate the OPL image. First the lines of minimum intensity parallel to the fringe pattern are identified. Next, for each row of pixels, intensities (I_{ij}) between adjacent lines of minimum intensity (n and $n + 1$) were converted to differences in optical path length (D_{ij}):

$$D_{ij} = OPL_{ij} - \alpha_{ij}\lambda/2\pi = (\lambda/2\pi) \cdot \{\cos^{-1}[2(I_{ij} - I_{min(nj)})/(I_{max(nj)} - I_{min(nj)})] - 2\pi n\}, \quad (13)$$

where $I_{min(nj)}$ and $I_{max(nj)}$ are the intensity extrema of row j between adjacent lines of minimum intensity n and $n + 1$. The resulting map of optical path length difference (D_{ij}) is the sum of the optical path length due to the object (OPL_{ij}) and that arising from the manipulation of the reference beam by the plane parallel plates ($\alpha_{ij}\lambda/2\pi$). The contribution of the plates ($\alpha_{ij}\lambda/2\pi$) was computed by fitting a region of the map (D_{ij}) that did not contain cells (so that $OPL_{ij} = 0$) to a plane ($p_{ij} = p_1 i + p_2 j$). Because p is the best estimate of $-\alpha\lambda/2\pi$ obtained from the data, OPL_{ij} is determined by subtracting the values of the fitted plane (p_{ij}) from the OPL difference map:

$$OPL_{ij} = D_{ij} - p_{ij}. \quad (14)$$

Determination of cell volume and surface area

Using Eq. 1 (with $\gamma' = 0$ by referencing to the background), the computed OPL map and cell refractive index can be used to determine the cell height profile, $h(x, y)$, assuming that the refractive index of the cell is uniform. The cell height profile is then used to calculate cell volume

$$V = \iint_{cell} h(x, y)\, dx\, dy;$$

and cell surface area

$$A = \iint_{cell} dx\, dy + \iint_{cell} [1 + h_x^2(x, y) + h_y^2(x, y)]^{1/2}\, dx\, dy$$

(Amazigo and Rubenfeld, 1980). The first term in the surface area equation is the (flat) area of the base of the cells, the second integral represents the (curved) remainder of the surface, and $h_x(x, y)$ and $h_y(x, y)$ are the partial derivatives of $h(x, y)$ in the x and y directions, respectively. The integrations were carried out using the trapezoidal rule with definitions of the derivatives of the height profile accurate to second order (Press et al., 1988). The cell was defined as the region of contiguous points in the image that had height values greater than two standard deviations above the baseline.

Calculation of osmotic water permeability

The plasma membrane osmotic water permeability coefficient (P_f) was calculated from the time course of the interference signal of a cell layer in response to an imposed osmotic gradient. For a semipermeable membrane, P_f is related to volume change by

$$d(V/V_o)/dt = -P_f V_w (A/V_o)\Delta\Pi_o, \quad (15)$$

where $d(V/V_o)/dt$ is the initial rate of change of relative cell volume, A/V_o is the initial cell surface-to-volume ratio, V_w is the partial molar volume of water (18 cm^3/mol), and $\Delta\Pi_o$ is the initial osmotic gradient (outside-inside). A unity reflection coefficient is assumed for osmotically active solutes. The time course of relative volume change was calculated from a series of interference images by using Eq. 8.

For nonimaging interferometry, Eq. 9, 11, or 12 cannot in general be used to calculate the time course of relative volume change from the interference signal; instead Eq. 15 was used to generate a volume time course, and Eq. 12 with a measured cell height profile was used to convert the volume time course to an interference signal time course. The Levenberg-Marquart algorithm (Press et al., 1988) was used to fit the parameters (P_f, α_o, $d\alpha/dt$, E_{ro}, and E_{so}) that minimized χ^2 between the modeled interference signal time course and the data. All other parameters, including the height profile, were determined experimentally. Fitted $d\alpha/dt$, E_{ro}, and E_{so} values were generally within 30% of the values estimated from the experimental parameters.

RESULTS

Interference microscopy

Fig. 3 *A* shows an interference image of a test object consisting of a trapezoidal trough (height = 12.6 μm, width at base = 21.8 μm, width at top = 77.2 μm) cut in a glass slide (n = 1.515) filled with type FF immersion oil (n = 1.4789). The image analysis algorithm first identified the lines of minimum intensity (*thin white lines* in Fig. 3 *B*) and then used Eq. 13 to compute a map of the difference in optical path length between the object and the plane parallel plates (Fig. 3 *C*). The contribution of the plane parallel plates to the image was defined from the region in Fig. 3 *C* outside of the dashed box and was subtracted. The deduced OPL image of the object is shown in Fig. 3 *D*. The procedure generated OPL maps with low noise (standard deviation $\approx$ 15 nm) and flat background (Fig. 3 *E*). The calculated height profile of the object agreed with measurements of the real object made by confocal microscopy (*circles* in Fig. 3 *F*). The z-resolution of the interference microscope is limited by the standard deviation of the OPL image, which was typically $\lambda/50$ (see Discussion).

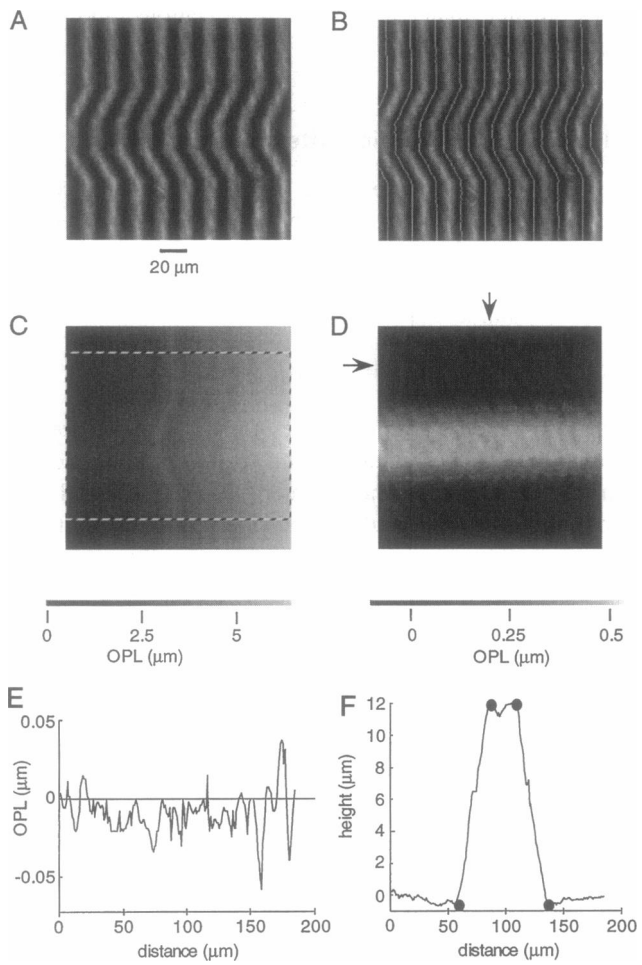

FIGURE 3 Analysis of interference image of a test object. (*A*) Interference image of a trapezoidal trough (height = 12.6 μm, width at base = 21.8 μm, width at top = 77.2 μm) cut in a glass slide (n = 1.515) filled with type FF immersion oil (n = 1.4789). (*B*) Lines of minimum intensity are shown as thin white lines. (*C*) The image in *B* was converted to a map of OPL using Eqs. 13 and 14. The data outside of the dashed box were used to estimate the contribution of the plane parallel plates. (*D*) OPL map after subtracting the contribution of the plane parallel plates. (*E*) Plot of the OPL of the background (intensities from horizontal line indicated by *arrow* in *D*). (*F*) Calculated height profile of the trough (*line*) (data from vertical line indicated by *arrow* in *D*). For comparison, the height of the object calculated by confocal microscopy (●) is shown.

Fig. 4 *A* shows an interference image of MDCK cells bathed in 300 mOsm (*top*) and 150 mOsm (*bottom*) perfusates of refractive index 1.3400. Cell volume should double if the MDCK cells respond as perfect osmometers. The vertical interference fringes were observed to shift as they crossed the cells. The deviations decreased as the cell volume increased, consistent with the predicted change in OPL through the cells. The OPL maps generated from the interference images are shown in Fig. 4 *B*. As cell volume increased, the OPL in the region of the cells decreased as predicted by Eq. 4. The cytoplasmic refractive index of the MDCK cells in 300 mOsm perfusate was measured to be 1.366 by immersion refractometry (Coble et al., 1982). Fig. 4 *C* shows the height profile of the cell at 300 mOsm calculated from the OPL image. The average cell height of 8.3 ± 0.7 μm (SE, n = 6 cells) was not significantly different ($p > 0.5$) from the value of 8.9 ± 0.7 μm (SE, n = 3) determined by confocal microscopy (data not shown). The average volume of an MDCK cell at 300 mOsm was 1.7 pl, and the surface-to-volume ratio was 6750 cm^{-1}. Cell volume increased by a factor of 1.8 when the perfusate osmolality was changed from 300 to 150 mOsm.

In the theory development, it was assumed that the cell refractive index was proportional to the relative osmolality of the extracellular medium (Eq. 3). To test this assumption, the refractive index of MDCK cells was measured by immersion refractometry at a series of perfusate osmolalities. Fig. 5 *A* shows a linear dependence of cytoplasmic refractive index on relative perfusate osmolality. The slope (0.0381 ± 0.0084) and y intercept (1.3284 ± 0.0057; SE, n = 12) of the least-squares linear fit to the data were not significantly different ($p > 0.1$) from the values assumed in Eq. 3 (slope = $(n_{cell} - n_w)$ = 0.0337; y intercept = n_w = 1.3323).

The theory predicts that for a fixed difference in cell volume, the difference in the integrated optical path length, $\Theta - \Theta_o$, is linearly proportional to the perfusate refractive index (Eq. 7). This prediction was tested in MDCK cells by measuring $\Theta - \Theta_o$ as the volume was increased by changing the perfusate osmolality from 300 to 150 mOsm. The refractive index of the perfusate was varied by the addition of dextran (1–5% w/v) to the perfusate. Fig. 5 *B* (representative of three sets of measurements) shows that $\Theta - \Theta_o$ was proportional to the perfusate refractive index. The x intercept (1.3312 ± 0.0013; SE, three sets of measurements) of the linear least-squares fit to the data was not significantly different ($p > 0.2$) from the predicted value, n_w = 1.3323. Together these results validate the model.

Interference microscopy was applied to measure plasma membrane osmotic water permeability in MDCK cell layers (Fig. 6). In response to a decrease in perfusate osmolality from 300 to 150 mOsm (at 24°C), cell volume progressively increased. Serial interference images were recorded and converted to OPL maps (representative images shown at top). Equation 8 was applied to generate from the OPL images the time course of relative cell volume (*circles* in Fig. 6). For comparison, data acquired by using TIR microfluorimetry on duplicate MDCK cell layers are shown. The perfusion exchange time was less than 1 s (data not shown). There was good agreement between the data acquired by interference microscopy (*circles*) and TIR microfluorimetry (*line*) (Farinas et al., 1995). As expected, cell volume approximately doubled. Using Eq. 15, the osmotic water permeability coefficient (P_f) was calculated to be 9×10^{-4} at 24°C, using a surface-to-volume ratio of 6750 cm^{-1} computed from the cell height profile shown in Fig. 4.

For nonimaging experiments (as in Fig. 2 *B*), the relationship between cell volume and interference signal amplitude is dependent upon cellular and experimental parameters (Eqs. 9, 11, and 12). The influence of these parameters

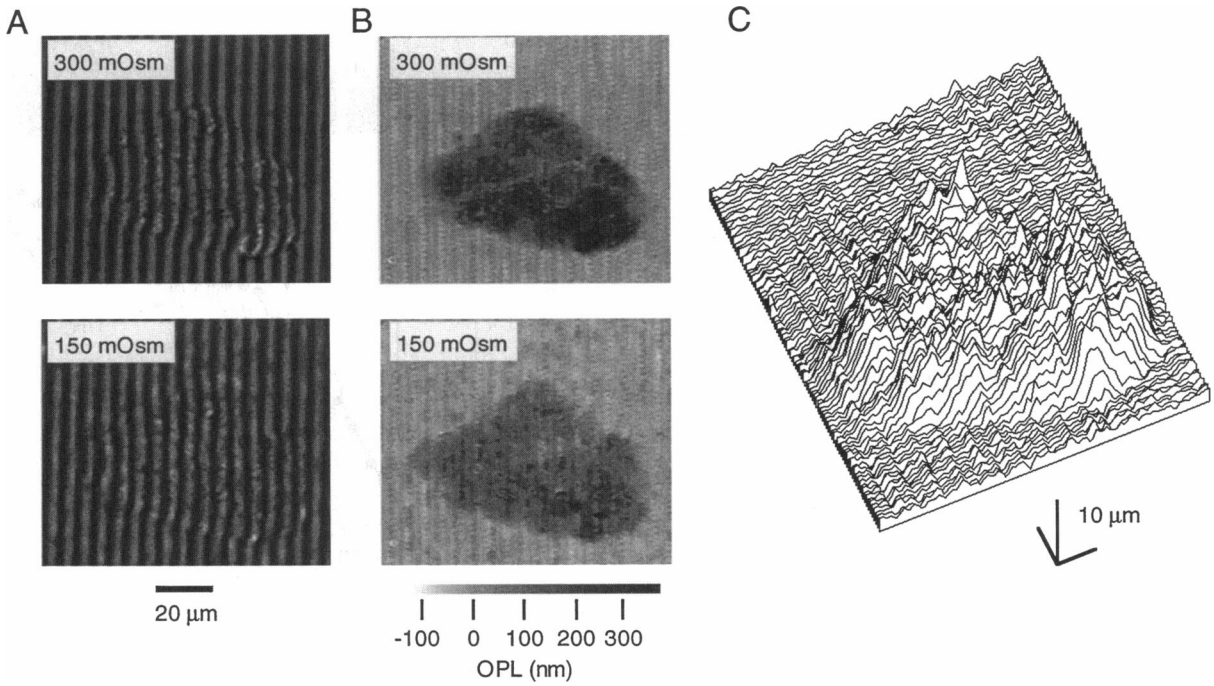

FIGURE 4 Cell volume change causes a change in optical path length. (*A*) Interference images of MDCK cells perfused with 300 (*top*) and 150 (*bottom*) mOsm solutions. (*B*) OPL maps calculated from the interference images of the cells. (*C*) Cell height profile calculated from the OPL images at 300 mOsm.

on the predicted signal was calculated from the theory and plotted as the interference signal as a function of relative cell volume (Fig. 7). For a flat epithelium of height $h_o = 20$ μm with refractive index difference $n_w - n_p = -0.03$, Eq. 9 predicts that a change in cell volume results in a substantial change in interference signal (Fig. 7 *A*). As the difference in refractive index between water and the perfusate decreases ($n_w - n_p = -0.01$) or as cell height decreases ($h_o = 10$ μm), the sensitivity of the interference signal to a change in cell volume decreases. The relative amplitude of the reference and sample beams (E_r/E_s) had a minor effect on the relationship between the interference signal and relative cell volume over a fivefold change in ratio (Fig. 7 *B*); only the scaling was affected. Fig. 7 *C* shows that the phase difference between the reference and sample beams, α, shifts the locations of the extrema but does not change the overall shape of the curve.

The effect of cell shape on the predicted signal was investigated for five model cell shapes: 1) flat cells ($h_o = h$, where h is the average cell height); 2) nearly flat cells with surface undulations ($h_o = h + \cos[x + y]$); 3) round cells ($h_o = 0.127h\ [h^2 - x^2]^{1/2}$); 4) flat cells with intercellular spaces ($h_o = h/0.95$ for 95% of the area and zero elsewhere); and 5) Gaussian-shaped cells ($h_o = h' \exp[-(x^2 + y^2)/w^2]$), where $h' = 4x_{max} \cdot y_{max}h/[\pi w^2 \mathrm{erf}(x_{max}/w)\mathrm{erf}(y_{max}/w)]$, h is the average cell height, and w is the width of the Gaussian. An average cell height of 10 μm, $\lambda = 633$ nm, $E_{ro} = E_{so}$, $\alpha = \pi/2$, and $n_p - n_w = -0.01$ were used for the computations shown in Fig. 7 *D*. The dependence of the interference signal on cell volume was relatively insensitive to cell shape, particularly for relative volumes near unity. The largest deviations from the response predicted for a flat epithelium occurred for cell shapes that have a wide distribution of cell heights, such as the Gaussian-shaped cells.

To investigate the effect of nonuniform changes in cell shape with changes in cell volume [$h(x, y) \neq h_o(x, y)V/V_o$], the predicted dependence of interference intensity on relative cell volume was calculated for Gaussian-shaped cells ($h = h' \exp[-(x^2 + y^2)/w^2]$, where w is a function of relative volume (see figure legend) and compared to flat cells and to Gaussian-shaped cells that undergo uniform shape changes. As seen in Fig. 7 *E*, even for cells that undergo shape change during volume change, the response was similar to that for a flat epithelium. Taken together, the calculations indicate that small changes in relative cell volume lead to large changes in interference signal, and that the relationship between signal and cell volume is relatively insensitive to the details of cell shape and various instrument parameters.

Nonimaging interferometry measurements of water permeability were conducted with MDCK monolayers. In the absence of a cell layer in the flow chamber, exchanging perfusates between PBS ($n = 1.3341$) and PBS containing 5% (w/v) dextran ($n = 1.3405$) produced multiple maxima and minima in the interference signal (Fig. 8 *A*). The curve at the bottom shows that the corresponding change in optical path length had a half-time for fluid exchange of ~6 s. In contrast, when perfusate osmolality was switched from 300 to 150 mOsm at a constant refractive index (solutions matched to better than 20 ppm), there was little change in

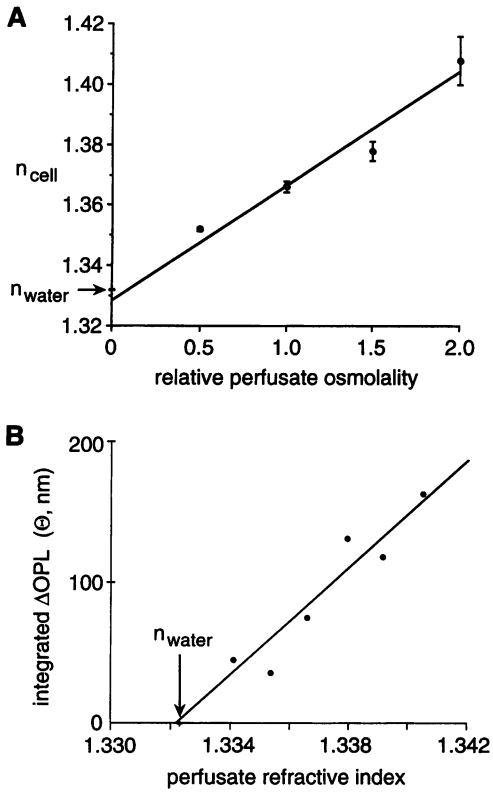

FIGURE 5 Validation of model predictions. (*A*) The cytoplasmic refractive index of MDCK cells was measured by immersion refractometry after equilibrating cells at 150, 300, 450, and 600 mOsm (see Eq. 2). Points are plotted as the mean ± SE of three or four measurements. (*B*) The difference in integrated optical path length, $\Theta - \Theta_o$, after a doubling of cell volume (cells switched from 300 to 150 mOsm perfusate) as a function of perfusate refractive index (see Eq. 7), adjusted by the addition of dextran (1–5% w/v). See text for explanations.

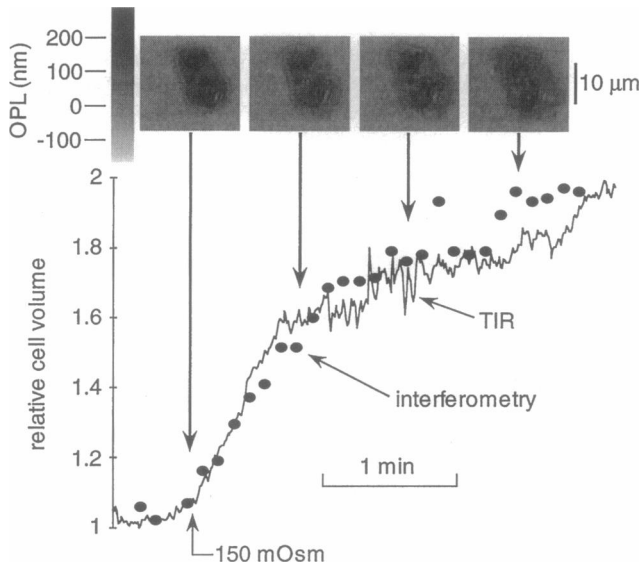

FIGURE 6 Plasma membrane osmotic water permeability of an MDCK cell layer. Serial interference images were acquired in response to a change in perfusate osmolality from 300 to 150 mOsm at 24°C. After converting the images to OPL maps (representative maps shown at *top*), the integrated optical path length was converted to relative cell volume (●) using Eq. 8. For comparison, data acquired by TIR microfluorimetry are shown (*solid line*). Fitted P_f values are given in the text.

interference signal, except for a small transient signal at the time of solution exchange (Fig. 8 *B*, *top*). In the presence of an MDCK cell monolayer, the identical change in perfusate solutions produced a time-dependent change in interference signal (Fig. 8 *B*, *bottom*). The best fit to the data gave a P_f value of 4.8×10^{-4} cm/s (see legend) (*dashed curves* shown in Fig. 8 *B*). The average P_f value of $6.1 \pm 2 \times 10^{-4}$ cm/s (SE, $n = 4$) at 24°C agreed with that obtained by both interference microscopy and TIR microfluorimetry. The theory-based curve fit the experimental data very closely.

Nonimaging interferometry was used to measure the luminal plasma membrane osmotic water permeability of toad urinary bladder epithelium. In the unstimulated epithelium, a change in perfusate osmolality from 240 to 120 mOsm resulted in a slow change in interference signal (Fig. 8 *C*, *top*). From the fit to the data, a P_f value of 0.009 cm/s was calculated. After incubation with 50 μM forskolin, the same change in perfusate osmolality caused a more rapid change in interference signal (Fig. 8 *C*, *bottom*). The results of the fit to the data indicate that forskolin addition increased apical membrane water permeability by fivefold to 0.04 cm/s at 23°C.

DISCUSSION

The goal of this study was to develop a method to measure plasma membrane osmotic water permeability in planar sheets of epithelial cells. As explained in the introduction, the existing methods of measuring water permeability are not suitable for studies in nonadherent cell sheets. Our strategy was to utilize interferometry to quantify the small change in the optical path length of a laser beam passing through a cell as cell volume changes. Osmotic water permeability was then measured from the time course of cell volume in response to osmotic gradients imposed by changing solutions bathing the cell surface. Interference microscopy with image analysis was first used to validate the theory relating cell shape to interference signal amplitude, and to measure water permeability in MDCK epithelial cells. Analysis of interference images permitted the mapping of cell height in living cells with a z-resolution better than that obtainable by confocal microscopy, but not as good as that for determination of the z-position of a single small fluorescent bead (Kao and Verkman, 1994).[2] Whereas the resolution in confocal microscopy is limited by the diffraction of light, the resolution of height in the interfer

[2] The z-resolution is defined as the smallest change in height that can be statistically distinguished—twice the noise of a height measurement. In a typical image (Fig. 4 *C*), the noise was 150 nm as determined from the standard deviation of an area of the image corresponding to a flat background. Because noise is inversely proportional to the square root of the number of observations, the z-resolution can be significantly improved by averaging pixels within an image or averaging several separate images.

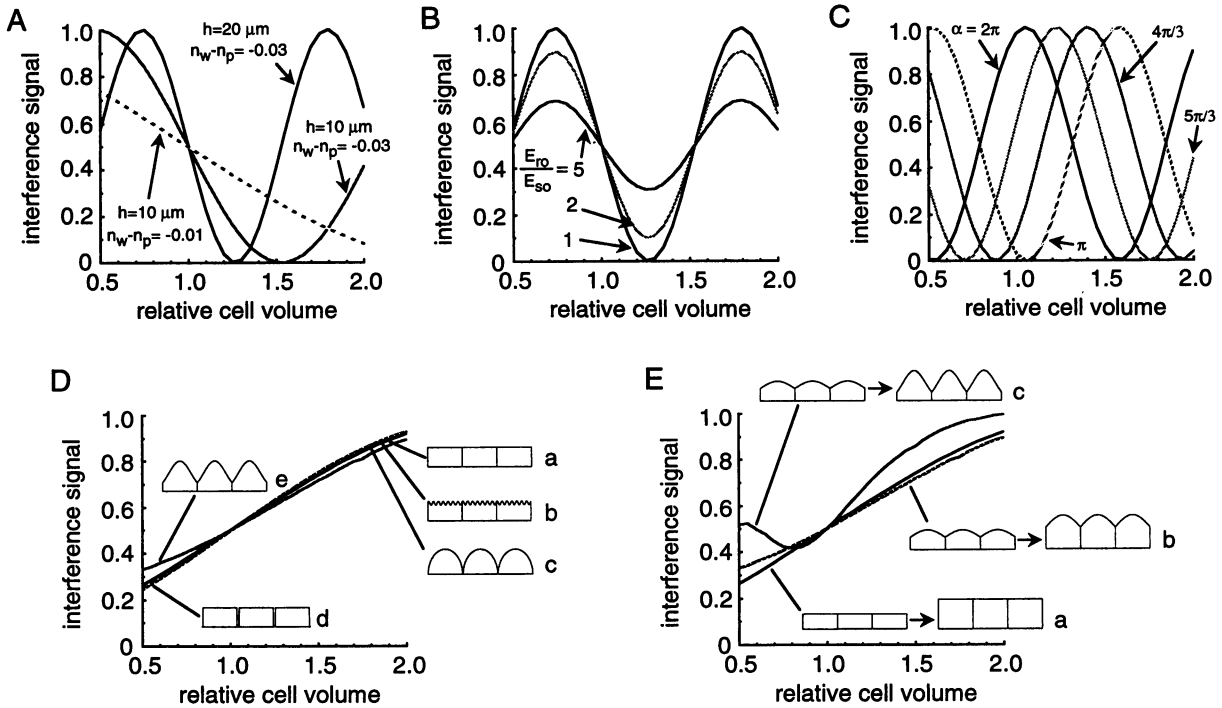

FIGURE 7 Theoretical predictions for nonimaging interferometry experiments. Interference signal intensity is plotted as a function of relative cell volume. (*A*) Sensitivity to the difference between the cell and perfusate refractive indices ($n_{cell} - n_p$) and cell height (h) (computed from Eq. 9, λ = 633 nm, $E_{ro} = E_{so} = 0.707$, $\alpha = \pi/2$, h and $n_w - n_p$ as indicated). (*B*) Sensitivity to the ratio of reference and sample beam amplitudes (E_r/E_s) (Eq. 9, λ = 633 nm, $E_{ro} + E_{so} = 0.707$, $\alpha = \pi/2$, h = 20 μm, $n_w - n_p = -0.03$, E_r/E_s as indicated). (*C*) Effect of the phase of the reference beam, α (Eq. 9, λ = 633 nm, $E_{ro} = E_{so} = 0.707$, h = 20 μm, $n_w - n_p = -0.03$, α as indicated). (*D*) Influence of cell shape for five shapes. *a*, Flat epithelium ($h_o = h$); *b*, nearly flat epithelium (h_o = h + cos[$x + y$]); *c*, round cells ($h_o = 0.127\ h[h^2 - x^2]^{1/2}$); *d*, square cells with an intercellular space ($h_o = h/0.95$ for 95% of the area and zero elsewhere); *e*, Gaussian-shaped cells ($h_o = h' \exp[-(x^2 + y^2)/w^2]$), where h is the average cell height, $h' = 4x_{max}y_{max}h/[w^2\pi\text{erf}(x_{max}/w)\text{erf}(y_{max}/w)]$, and w is the width of the Gaussian (h = 10 μm, λ = 633 nm, $E_{ro} = E_{so}$, $\alpha = \pi/2$, $n_p - n_w = -0.01$). (*E*) The effect of nonuniform cell shape change. *a*, Flat cells; *b*, Gaussian-shaped cells that undergo uniform shape change, as above; and *c*, Gaussian-shaped cells ($h = h' \exp[-(x^2 + y^2)/w^2]$), where w is a function of relative volume (V/V_o) such that $\int\int h(w)\,dx\,dy/\int\int h(w_o)\,dx\,dy = V/V_o$. The cross-sectional shape of the cells is shown schematically.

ence microscope is not limited by diffraction but only by measurement noise. A Mach-Zehnder interferometer was then constructed, and the theory was developed to measure osmotic water permeability in cell sheets without microscopy and image analysis. Nonimaging interferometry was used to measure the plasma membrane water permeability of MDCK cell layers and the intact toad urinary bladder.

There are a number of technical considerations in the application of interferometry to the measurement of cell volume. For microscopy with image analysis, an interference microscope is required. In addition, quantitative image analysis requires adequate pixel resolution and excellent linearity, like that afforded by a 14-bit CCD camera detector. In the studies performed here, a costly Leitz interference microscope was used that contained optics to closely match the reference and sample optical path lengths. The microscope was constructed before the wide availability of coherent light sources. With the use of modern ion lasers or laser diode sources with a coherence length of >10 cm, it is possible to modify a standard, single-objective, transmission light microscope to perform interference measurements. The coherent illumination source is split into a sample beam that passes through the microscope condenser and objective, and an external reference beam, which are recombined to create interference fringes. Because imaging is required, the data acquisition rate is limited by the camera frame acquisition rate (~1 s), so imaging interferometry is not suitable for measuring very fast changes in cell volume.

Nonimaging interferometry can be utilized if single-cell measurements and cell shape reconstructions are not needed. The approach described here used a Mach-Zehnder interferometer to record the intensity of the zeroth-order interference fringe. It was shown theoretically that the intensity of the zeroth-order fringe provided information about average relative cell volume. For nonimaging interferometry any cell layer that is not flat leads to scattering of the incident laser beam. This is problematic because each part of the beam will travel through a different optical path length. If the sample and reference beam interference were measured in the near-field limit, the differences in optical path length would lead to a complex average interference signal. In contrast, by measuring the interference of the

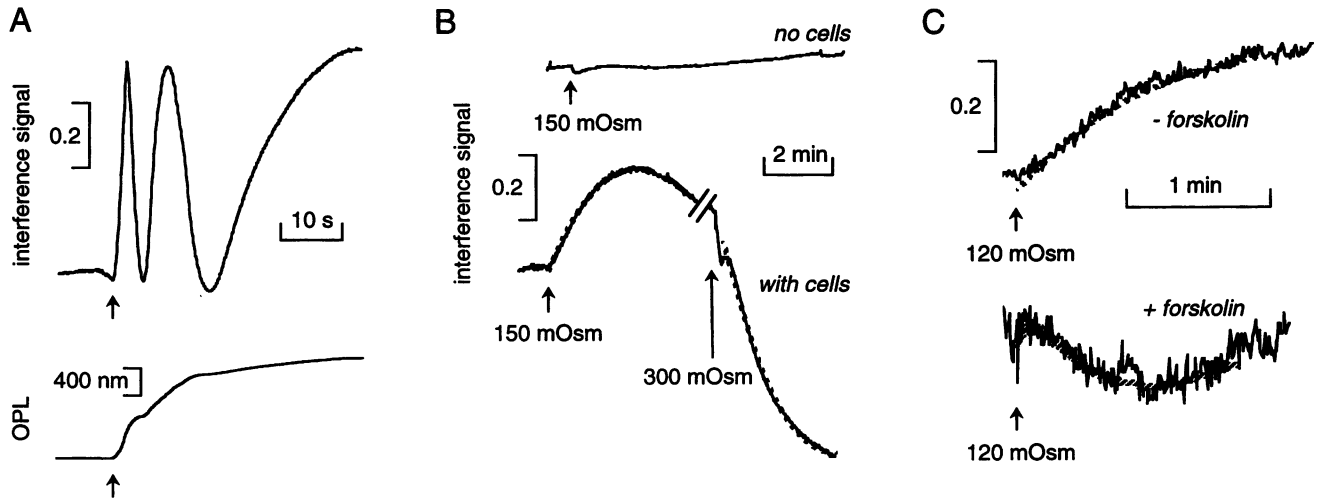

FIGURE 8 Nonimaging interferometry of epithelial cells. (*A*) The interference signal was recorded in the absence of cells in response to a change in perfusate refractive index (1.3341 to 1.3405) at constant osmolality (*top*); the deduced time course of optical path length is shown at the bottom. (*B*) The interference signal was recorded in the absence of cells with a change of perfusate osmolality (300–150 mOsm) at constant refractive index (1.3405) (*top*), and in the presence of an MDCK cell layer after changing perfusate osmolality from 300 to 150 mOsm and back to 300 mOsm (*bottom*). The dashed curve is the best fit obtained as described in Theory and Data Analysis, with $P_f = 4.8 \times 10^{-4}$ cm/s, $\alpha_o = 0.7$ rad, $d\alpha/dt = 0.006$ rad/s, $E_{ro} = 0.23$ and $E_{so} = 0.1$ (300 to 150 mOsm), and $P_f = 4.9 \times 10^{-4}$ cm/s, $\alpha_o = 0.9$ rad, $d\alpha/dt = -0.01$ rad/s, $E_{ro} = 0.19$ and $E_{so} = 0.11$ (150 to 300 mOsm). Average fitted P_f values are given in the text. (*C*) The interference signal was recorded for toad bladder epithelium with a change in perfusate osmolality from 240 to 120 mOsm at constant refractive index (1.3400) before forskolin stimulation (*top*) and after incubation with 50 μM forskolin for 10 min. The dashed curve is the best fit with $P_f = 0.009$ cm/s, $\alpha_o = 0.8$ rad, $d\alpha/dt = -0.002$ rad/s, $E_{ro} = 0.15$, and $E_{so} = 0.09$ (− forskolin) and $P_f = 0.04$ cm/s, $\alpha_o = 3$ rad, $d\alpha/dt = -0.003$ rad/s, $E_{ro} = 0.12$, and $E_{so} = 0.10$ (+ forskolin). The surface-to-volume ratio was taken as the reciprocal average cell height of 12.5 μm.

beams in the far-field limit, the theory predicts the dependence of interferometric signal on cell volume.

We found that both the single-pass (Mach-Zehnder) and double-pass (Michelson) interferometry configurations produced adequate interference signals for the measurement of water permeability in cell layers (data for Michelson interferometer not shown). The Mach-Zehnder configuration, in which the sample beam traversed the cell layer only once, was used for further studies because of the relatively simplified mathematical analysis (Eqs. A1–A8) to relate the interference signal amplitude to averaged cell volume. An objective lens was used to expand the interference profile to enable detection of the (far-field) zeroth-order fringe. It is noted that the interference signal amplitude was very sensitive to small changes in temperature, and to air currents and vibration; for example, the refractive index of water changes by 200 ppm for a 1°C change in temperature. For this reason, the interferometer was enclosed in an air-tight lucite box in a dark room at constant temperature, and positioned on an antivibration optical table. Solutions entering the perfusion chamber were passed through a coil immersed in a constant temperature bath. Finally, the precise matching of solution refractive index to better than 20 ppm was required to avoid transients in interference signal amplitude due to solution exchange.

Although interferometry has been widely utilized in the physical sciences for measurements requiring extreme precision, ranging from the Michelson-Morley experiment, which showed that there is no luminiferous aether, to the planned LIGO gravity wave observatory, there have been few applications in the biological sciences. Early attempts to apply interference microscopy to biology focused on measurement of the solids content of various cell types (Allen and Francis, 1966; Barer and Dick, 1957). The osmolality of the intercellular space in *Necturus* gallbladder was estimated by using interference microscopy, but the limited measurement precision did not allow resolution of the standing gradient hypothesis for near-isosmotic transport (Coble et al., 1982). Recently, the high precision attainable by interferometry was used to measure the step size of single kinesin motor proteins (Svoboda et al., 1993).

In summary, an interferometry method was developed and validated that allowed the measurement of the plasma membrane osmotic water permeability coefficient of intact epithelia. Changes in cell volume can be measured with excellent temporal resolution. The P_f value measured for MDCK cell layers was consistent with measurements by TIR microfluorimetry. The low permeability of MDCK cells is consistent with the absence of known water channels on the plasma membrane. The experiments with the toad urinary bladder epithelium demonstrated the ability to measure water permeability of an intact epithelium. The fivefold increase in P_f upon forskolin stimulation is consistent with the increase in transepithelial water transport previously reported (transepithelial $P_f = 0.028$ cm/s; Shi et al., 1990). The measured water permeability of the apical membrane after forskolin stimulation (0.04 cm/s) was comparable to that of 0.02 cm/s estimated by analysis of images acquired ~10 s apart (Kachadorian et al., 1985). When water channel knock-out transgenic mice become available, the interfero

metric method should be useful for defining the physiological role of water channels in intact epithelia.

APPENDIX

For nonimaging interferometry of an epithelium that is not flat, the laser beam directed onto the sample is scattered so that the electric field amplitude at the detector is no longer given by $E_s = E_{so}\cos[\omega t - kr - (2\pi/\lambda)\,\mathrm{OPL}(x, y)]$. Because the detection plane is far from the scattering plane (distance > aperture size squared/λ), the electric field of the sample beam at the detector plane is given by the Fraunhoffer approximation (Hecht, 1987):

$$E_s(X, Y) = \mathrm{Re}[\exp\{i(\omega t - kR)\}\mathcal{F}\{Q(x, y)\exp[i(2\pi/\lambda)(\mathrm{OPL})]\}], \quad \text{(A1)}$$

where X and Y are the coordinates in the diffraction plane, Re[ ] denotes the real part of the function, $\mathcal{F}\{\}$ denotes the Fourier transform, $Q(x, y) = A_o\exp[-\pi(x^2 + y^2)/d^2]$ is the intensity aperture function for a Gaussian laser beam, and

$$A_o = E_{so}\Big/\iint_{\text{aperture}} dx\,dy.$$

Eq. A1 can be simplified when the size of the aperture, d, is very large compared to cell size:

$$E_s(X, Y) \approx \mathrm{Re}[\exp\{i(\omega t - kR)\}A_o\mathcal{F}\{\exp[i(2\pi/\lambda)(\mathrm{OPL})]\}]. \quad \text{(A2)}$$

Because the detector is at the origin of the far-field diffraction plane (Fig. 2 *B*), E_s is sampled at the origin:

$$E_s(0, 0) = \mathrm{Re}\left[E_{so}\exp\{i(\omega t - kR)\}\iint_{\text{aperture}}\exp\{i(2\pi/\lambda)(\mathrm{OPL})\}\,dx\,dy\Big/\iint_{\text{aperture}} dx\,dy\right]. \quad \text{(A3)}$$

For a nearly flat epithelium, $\mathrm{OPL}(x, y) = \gamma + \mathrm{OPL}'(x, y)$, where $\mathrm{OPL}'(x, y) < \lambda/2\pi$. Approximating $\exp\{i(2\pi/\lambda)(\mathrm{OPL})\}$ by the first two terms of the Taylor's series expansion: $\exp\{i(2\pi/\lambda)(\mathrm{OPL})\} \approx \exp\{i(2\pi/\lambda)\gamma[1 + i(2\pi/\lambda)(\mathrm{OPL}'(x,y))]\}$, Eq. A3 becomes

$$E_s(0, 0) = E_{so}\,\mathrm{Re}[(\exp\{i(\omega t - kR)\}\exp\{i(2\pi/\lambda)\gamma\}\cdot(1 + i(2\pi/\lambda)\Theta')], \quad \text{(A4)}$$

where

$$\Theta' = \iint_{\text{aperture}}(2\pi/\lambda)(\mathrm{OPL}')\,dx\,dy\Big/\iint_{\text{aperture}} dx\,dy.$$

Approximating $\tan^{-1}\Theta' \approx \Theta'$ for small Θ', Eq. A4 becomes

$$E_s(0, 0) = \cos(\omega t - kR - \Theta). \quad \text{(A5)}$$

After interference of the sample beam (Eq. A5) with the reference beam (per Eq. 11), the intensity at the detector is

$$I(0, 0) = E_{ro}^2/2 + E_{so}^2/2 + E_{ro}E_{so}\cos[(2\pi/\lambda)\Theta - \alpha]. \quad \text{(A6)}$$

For an epithelium of arbitrary shape, Eq. A3 can be rewritten:

$$E_s(0, 0) = E_{so}[\cos(\omega t - kR)\,C - \sin(\omega t - kR)\,S], \quad \text{(A7)}$$

where

$$C = \iint_{\text{cell}}\cos[(2\pi/\lambda)\mathrm{OPL}(x, y)]\,dx\,dy\Big/\iint_{\text{cell}} dx\,dy \text{ and}$$

$$S = \iint_{\text{cell}}\sin[(2\pi/\lambda)\mathrm{OPL}(x, y)]\,dx\,dy\Big/\iint_{\text{cell}} dx\,dy.$$

After interference with the reference beam, the intensity at the detector is

$$I(0, 0) = E_{ro}^2/2 + E_{so}^2/2[C^2 + S^2] + E_{ro}E_{so}[\cos(\alpha)\,C + \sin(\alpha)\,S]. \quad \text{(A8)}$$

For a specified cell shape, Eq. A7 or A8 relates cell volume to interference intensity.

We thank Ulrike DeMarco for cell culture, Dr. Neil Emans for providing the toad bladders, Dr. Ken Spring for useful discussions regarding interference microscopy and for providing the interference microscope, and Dr. Alex Farinas for invaluable advice on interferometry.

This work was supported by grants DK35124, HL42368, and DK43840 from the National Institutes of Health. JF was supported by a predoctoral fellowship from the American Heart Association, California Affiliate, and a grant from the Achievement Rewards for College Scientists Foundation.

REFERENCES

Allen, R., and D. Francis. 1966. Cytoplasmic contraction and the distribution of water in the amoeba. *J. Exp. Biol.* 17:259–271.

Amazigo, J., and L. Rubenfeld. 1980. Advanced Calculus and Its Applications to the Engineering and Physical Sciences. John Wiley and Sons, New York.

Barer, R., and D. Dick. 1957. Interferometry and refractometry of cells in tissue culture. *Exp. Cell Res. Suppl.* 4:103–135.

Coble, A., J. Leader, and K. Spring. 1982. Microscope Interferometry of Necturus Gallbladder Epithelium in the Paracellular Pathway: Report of a Conference. Stanley E. Bradley and Elizabeth F. Purcell, editors. Independent Publishers Group, New York. 270–303.

Crowe, W. E., J. Altamirano, L. Huerto, and F. J. Alvarez-Leefmans. 1995. Volume changes in single N1E-115 neuroblastoma cells measured with a fluorescent probe. *Neuroscience.* 69:283–296.

Deen, P., M. Verdijk, N. Knoers, B. Wieringa, L. Monnens, C. van Os, and B. van Oost. 1994. Requirement of human renal water channel aquaporin-2 for vasopressin-dependent concentration of urine. *Science.* 264: 92–95.

Echevarria, M., and A. S. Verkman. 1992. Optical measurement of osmotic water transport in cultured cells: evaluation of the role of glucose transporters. *J. Gen. Physiol.* 99:573–589.

Farinas, J., V. Simenak, and A. S. Verkman. 1995. Cell volume measured in adherent cells by total internal reflection microfluorimetry: application to permeability in cells transfected with water channel homologs. *Biophys. J.* 68:1613–1620.

Fischbarg, J., J. Li, K. Kuang, M. Echevarria, and P. Iserovich. 1993. Determination of volume and water permeability of plated cells from measurements of light scattering. *Am. J. Physiol.* 265:C1412–C1423.

Folkesson, H. G., M. Matthay, A. Frigeri, and A. S. Verkman. 1996. Transepithelial water permeability in microperfused distal airways. Evidence for channel-mediated water transport. *J. Clin. Invest.* 97: 664–671.

Hecht, E. 1987. Optics. Addison-Wesley Publishing Company, Menlo Park, CA.

Kachadorian, W., S. Sariban-Sohraby, and K. Spring. 1985. Regulation of water permeability in toad urinary bladder at two barriers. *Am. J. Physiol.* 253:F120–F125.

Kao, H. P., and A. S. Verkman. 1994. Tracking of single fluorescent particles in three dimensions: use of cylindrical optics to encode particle position. *Biophys. J.* 67:1291–1300.

Katsura, T., J. M. Verbavatz, J. Farinas, T. Ma, D. A. Ausiello, A. S. Verkman, and D. Brown. 1995. Constitutive and regulated membrane expression of aquaporin 1 and aquaporin 2 water channels in stably transfected LLC-PK1 epithelial cells. *Proc. Natl. Acad. Sci. USA.* 92: 7212–7216.

Muallem, S., R. Zhang, P. A. Loessberg, and R. A. Star. 1992. Simultaneous recording of cell volume changes intracellular pH or Ca^{2+} concentration in single osteosarcoma cells UMR-106-01. *J. Biol. Chem.* 267:17658–17664.

Nielsen, S., and P. Agre. 1995. The aquaporin family of water channels in kidney. *Kidney Int.* 48:1057–1068.

Press, W., B. Flannery, S. Teukolsky, and W. Vetterling. 1988. Numerical Recipes in C. Cambridge University Press, Cambridge, England.

Shi, L. B., Y. Wang, and A. S. Verkman. 1990. Regulation of the formation and water permeability of endosomes from toad bladder granular cells. *J. Gen. Physiol.* 96:789–808.

Svoboda, K., C. Schmidt, B. Schnapp, and S. Block. 1993. Direct observation of kinesin stepping by optical trapping interferometry. *Nature.* 365:721–727.

Verkman, A. S. 1995. Optical methods to measure membrane transport processes. *J. Membr. Biol.* 148:99–110.

Verkman, A. S., A. N. van Hoek, T. Ma, A. Frigeri, W. R. Skach, A. Mitra, B. K. Tamarappoo, and J. Farinas. 1996. Water transport across mammalian cell membranes. *Am. J. Physiol.* C12–C30.